Supplementary Figures

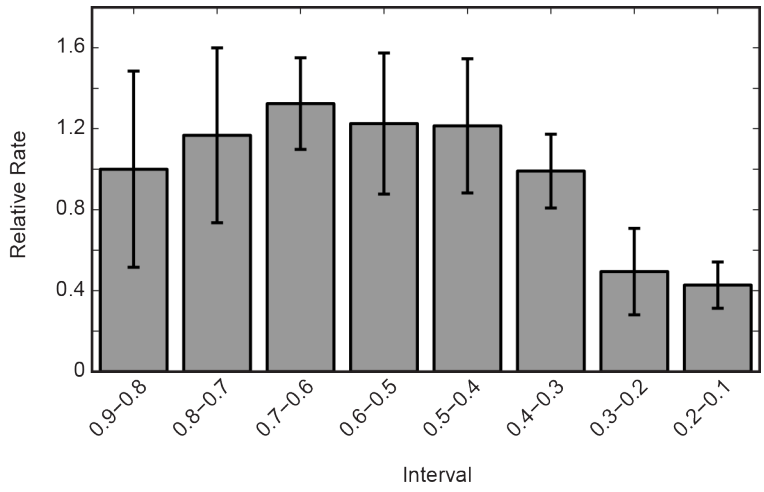

Supplementary Figure S1: Relative average rate as compaction progresses.

The compaction rate is relatively steady over the course of a condensation experiment, but slows down towards the end. Rate depicted relative to the rate in the interval of 0.9 to 0.8 of the original end-to-end distance as measured in the pre-measurement.

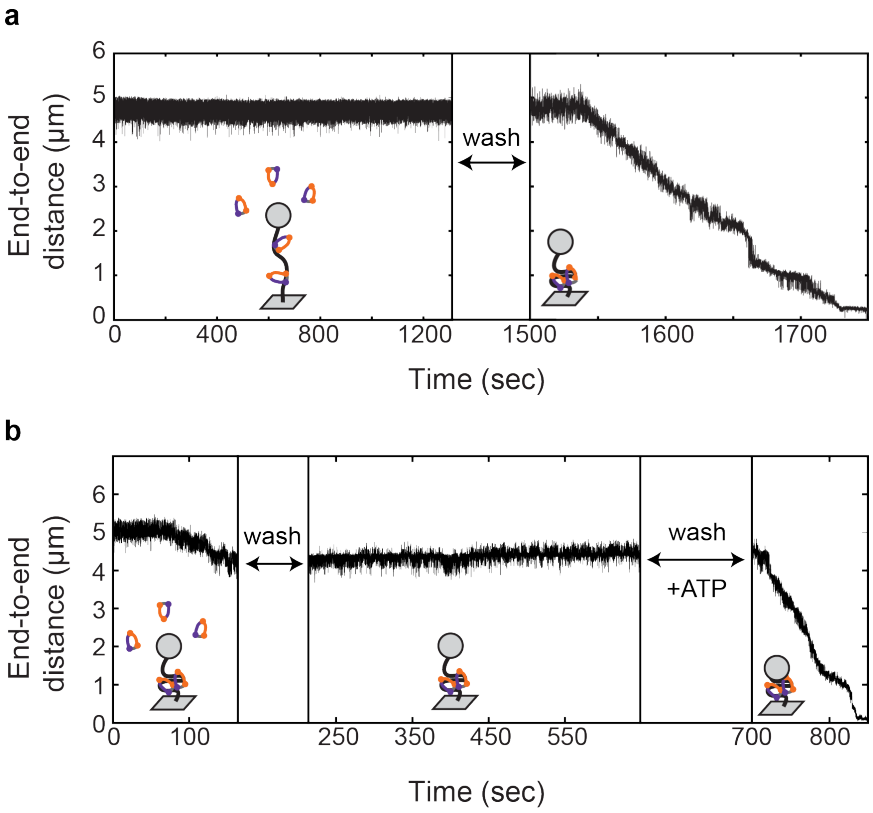

Supplementary Figure S2: Condensin does not compact DNA in the absence of ATP or at high salt.

a) Example trace of DNA when condensin is added in the absence of ATP. After a 20-minute incubation, no condensation is observed. After washing the flow cell with buffer with no additional protein (t=1300), ATP is added (t=1500) and compaction is observed, indicating protein was bound in the absence of ATP.

b) At t=0, condensin and ATP are added and compaction is initiated. We interrupt ongoing DNA compaction by flushing with buffer without ATP (t=150). The compacted DNA remains compacted after washing with buffer without extra protein or ATP. Addition of ATP is necessary for compaction to proceed (t=700).

a

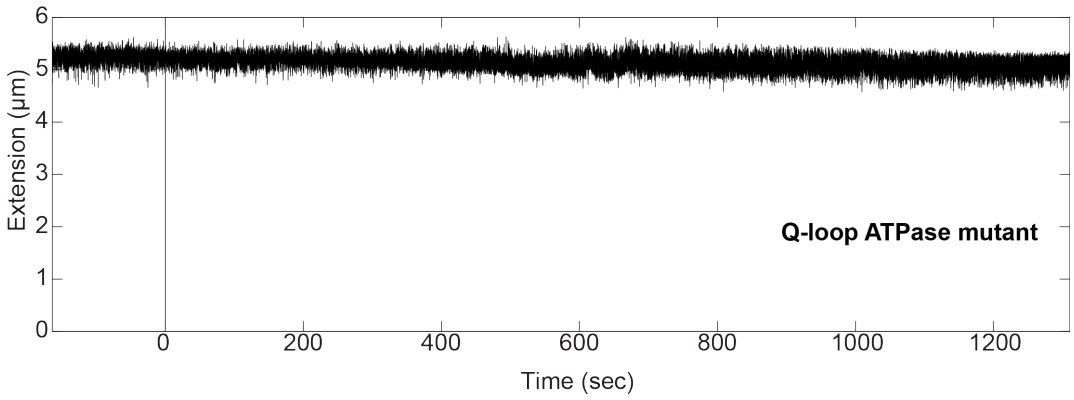

b

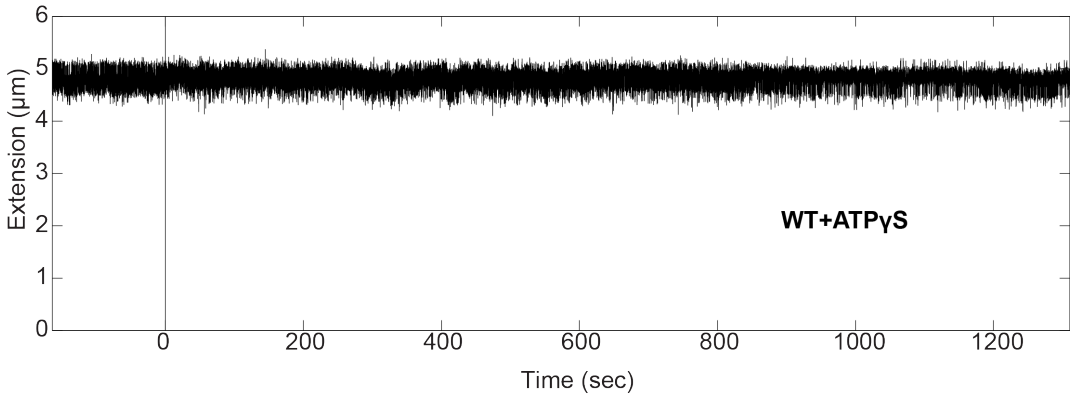

Supplementary Figure S3: Condensin ATPase mutant condensin, and wiltype protein+ATPγS do not compact DNA

a) Representative trace showing that the Q-loop condensin mutant does not compact DNA (N=12). Protein is added at t=0.

b) Representative trace showing that the wildtype condensin protein does not compact in the presence of ATPγS (N=11). Protein+ATPγS is added at t=0.

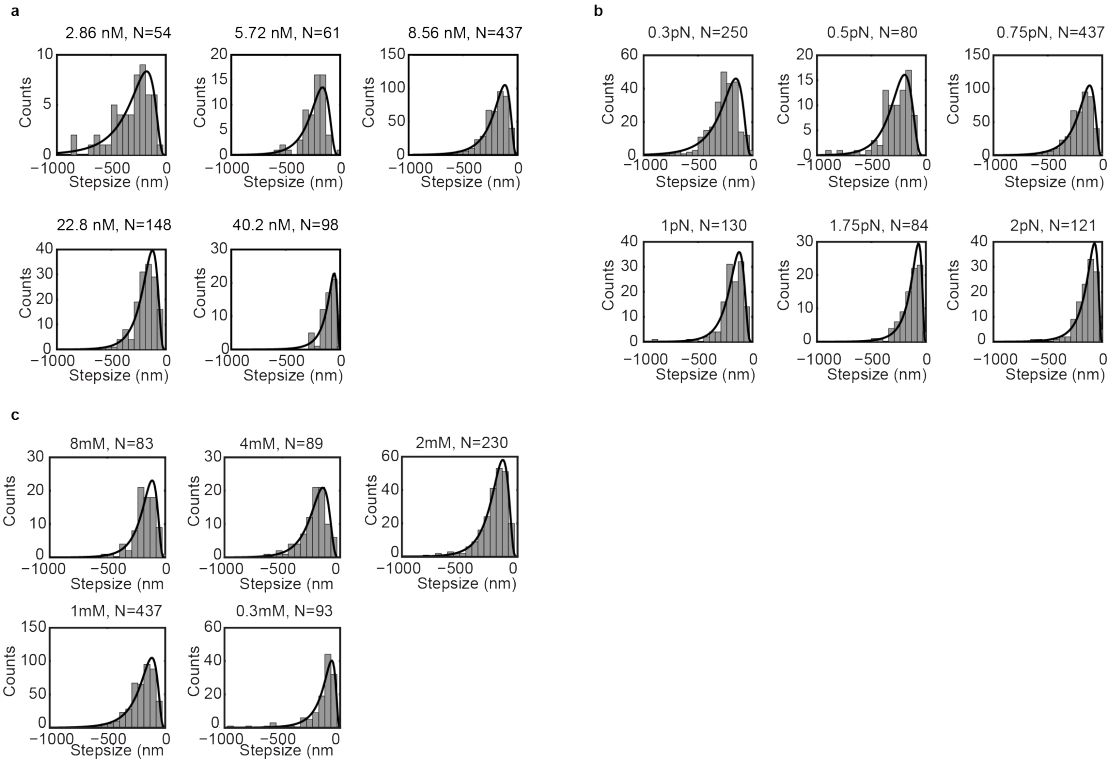

Supplementary Figure S4: Histograms of condensation step sizes for all conditions tested

a) Histograms for all protein concentrations. Lognormal distributions are fitted to negative steps.

b) Histograms for all ATP concentrations. Lognormal distributions are fitted to negative steps.

c) Histograms for all forces. Lognormal distributions are fitted to negative steps.

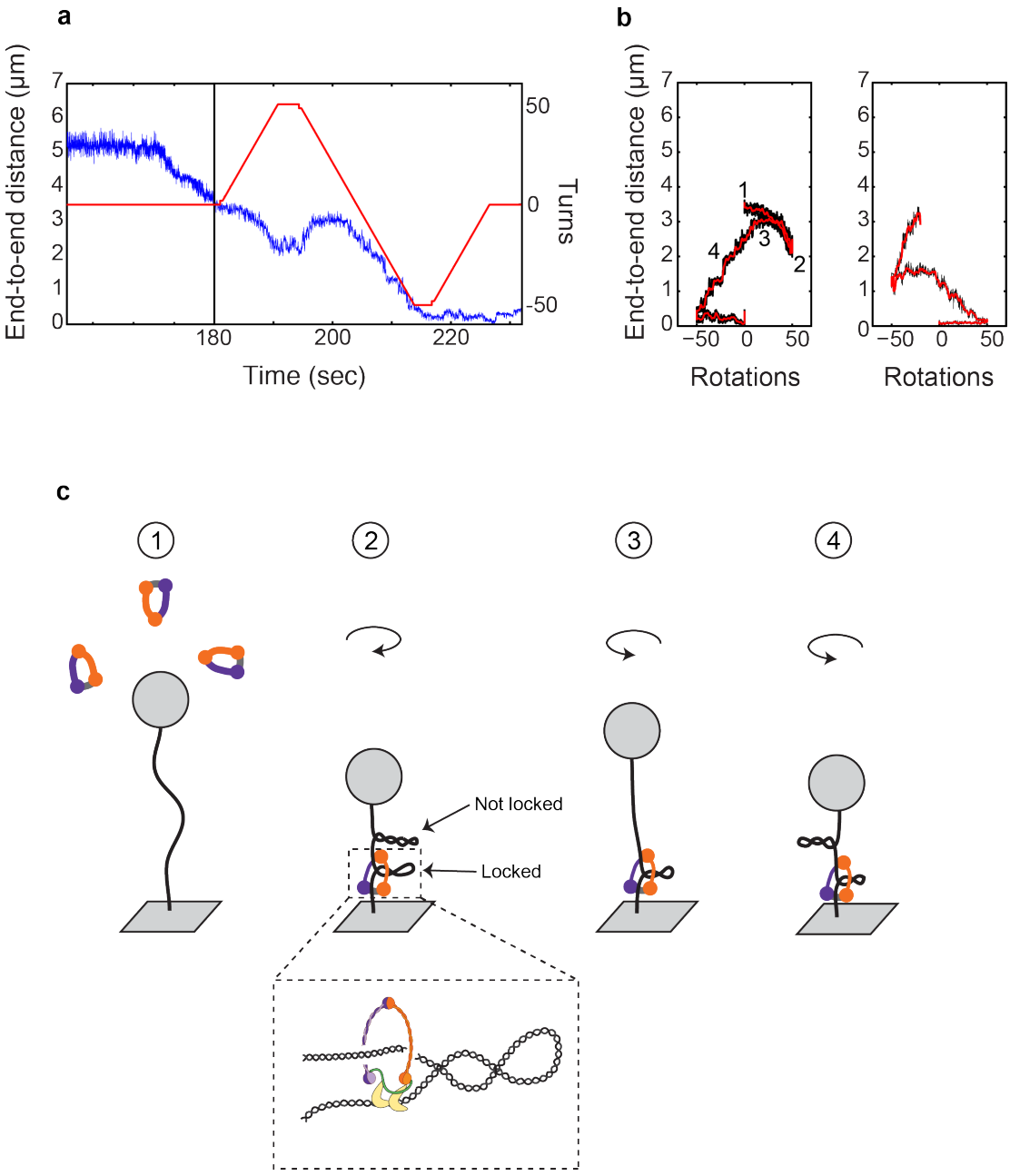

Supplementary Figure S5: Condensin shifts rotation curves.

a) Example of experiment with the compaction trace shown in blue and the rotations shown in red. Tether was compacted by condensin as usual. After about 50% condensation (at time=180), 50 positive rotations were applied. Then, the magnet was turned to -50 and back to 0.

b) Rotation curves of condensed DNA at 0.75pN. Left curve shows end-to-end length as a function of rotation, corresponding to the trace in Supplementary Figure 4a (after time=180). Right curve shows similar

experiment, only here negative turns were applied first. Numbers correspond to the states depicted in B.

c) Proposed model for condensation curve shifts in condensed molecules. We speculate that condensin is able to lock plectonemes. First, the DNA is “relaxed”, as no rotations are introduced yet. Second, the end-to-end length has decreased because 50 turns were absorbed (either positive or negative). Third, the turns are released as the magnet is rotating back to zero, but because condensin has “locked” some plectonemes, the end-to-end length of the DNA cannot be fully recovered. Instead, the rest of the DNA is essentially relaxed before reaching 0 turns. Therefore, the DNA starts absorbing the rotations, and end-to-end length is decreased again. In the shown examples, this shifts the highest point of the rotation curve from 0 to around 25, indicating that condensin has locked about 25 turns into a plectoneme. This process happens regardless of the initial rotation direction, suggesting that condensin can lock both positive and negative supercoils.

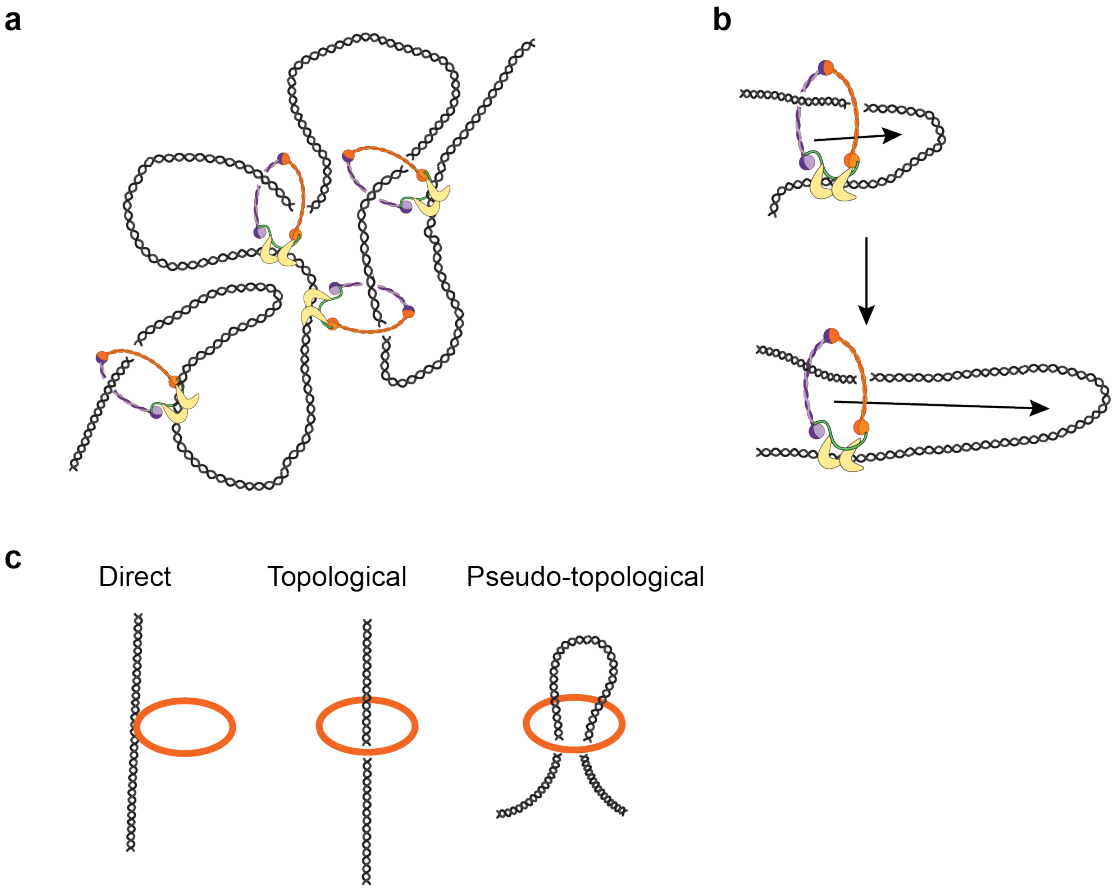

Supplementary Figure S6: Models for compaction.

a) The random-crosslinking model.

b) The loop-extrusion model.

c) Direct, topological, and pseudo-topological loading.

Supplemental methods

Step fitting analysis

We used a user-independent step-finding algorithm that was previously described and which has been abundantly used in many biological studies [1]. Briefly, the method works as follows. With this method, the best step fit is done based on least-square minimization. Then, the same number of steps is applied to the same data, but then deliberately misplaced, a so-called 'counter-fit'. The more prominent the steps are in a trace, the worse this counter fit is, i.e., the higher the chi-squared. For a featureless trace, the best and worst fit are not that different. Therefore, the ratio between residual chi-squared value of fit and counter-fit, maximizes at the most likely number of steps, whereas if there are no steps, this ratio is 1. In our analysis, we reject the fit if this ratio is below 1.15. Thus, as was shown before, by optimizing this parameter [1], the optimal fit is found as a function of the number of fitted steps.

For complicated step traces, this procedure tends to underestimate the number of steps. Therefore we perform a two-pass algorithm. To evaluate the variation of step sizes in an objective manner, we improved the implementation of this algorithm to allow for hands-off, batch style analysis. We follow an automated, three-phase analysis workflow:

1. We perform a "major step fit" as described above. Based on the individual errors for these fitted steps, we determine an "error-threshold".
2. This primary step fit is subtracted from the data. The residue may still contain smaller steps.
3. A "minor step fit" is performed on the residue with the same rejection criteria as for the first round, with the addition that the step errors need to be below the "error-threshold".
4. Finally, all accepted step locations are used to build the final fit. All these steps thus have similar error margins.

Figure S7 presents an example of the step fitting protocol.

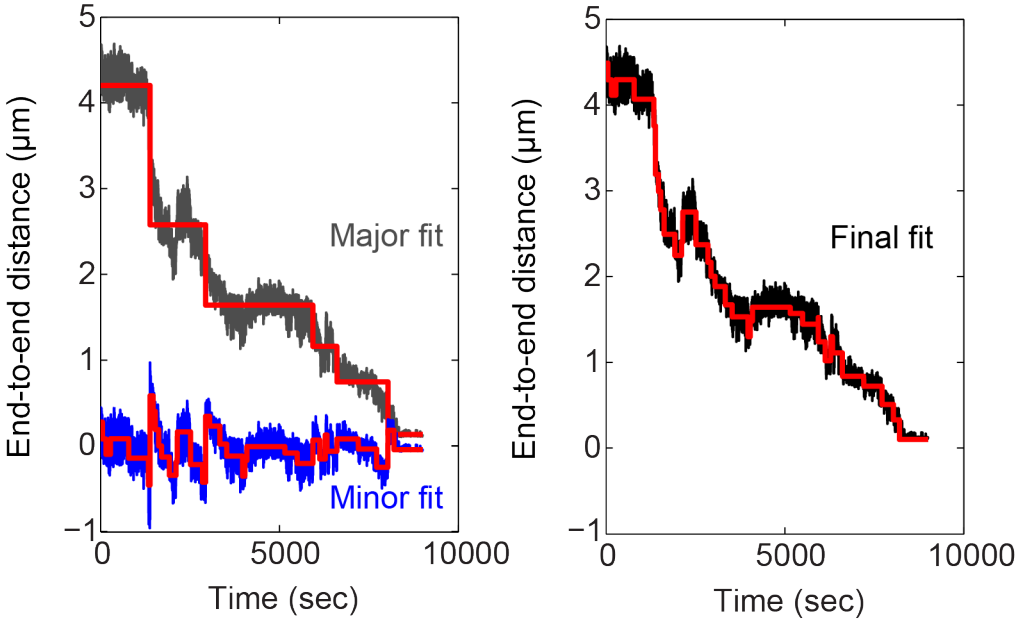

Supplementary Figure S7. Principle of multi-pass automated step fitting analysis.

First, a major step fit (upper red curve) is done on the data (left panel, gray). This fit is subtracted from the original data. Next, a minor step fit is done on the residue (left panel, blue). Accepted step fits are combined in a final fit (right panel).

Response time of the tethered bead.

In our magnetic tweezers, the magnetic bead cannot respond infinitely fast to an instant (condensation) step, since it is slowed down by the drag associated with moving the bead through the liquid. Here, we follow a simplified approach to obtain a ballpark estimate of the response time of the bead. This situation is reminiscent of the force-switch experiments performed by Crut et al[2].

We simplify the stretched DNA at an extension *e* as a linear spring with spring constant *k(e).* We also assume a mass-less, heavily overdamped system. For determining *k*, we assume the DNA behaves as a worm-like-chain. We expect the DNA to be stiffer after compaction, as the contour length is decreasing (Supplementary figure S8).

We start out with a stretched tether, where the magnetic force is balanced by the entropic stretching force of the DNA. Then, we assume that a condensation step instantly shortens the DNA by 200 nm. As the bead is initially still in the same position, the DNA is stretched by the same amount of 200 nm. During displacement of the bead following an instant shortening of the DNA, the drag force experienced by the bead is balanced with the DNA spring force:

$$F_{drag} + F_{spring} = 0 \text{ , or } \gamma \frac{dx}{dt} + \kappa x = 0$$

with $6\pi\eta r$ characterizing the Stokes drag of the bead, η the viscosity of water, and r the radius of the bead (0.5μm). The bead will therefore move according to

$$x(t) = x_0 e^{-t/\tau}$$

with $\tau = \frac{\gamma}{\kappa}$ the response time of the bead.

We evaluated the response time for three points: near the initial bare DNA extension at the applied pulling force (F=0.3pN, e=4.7μm), at halfway compaction (e=2.0μm), and at nearly complete compaction (e=0.6μm) (see Supplementary Figure S8). This yields values of k = $0.2145*10^{-6}$ to $0.8005*10^{6}$, leading to response times of τ = 100 to 400ms, respectively. This estimate is consistent with experimental measurements[2].

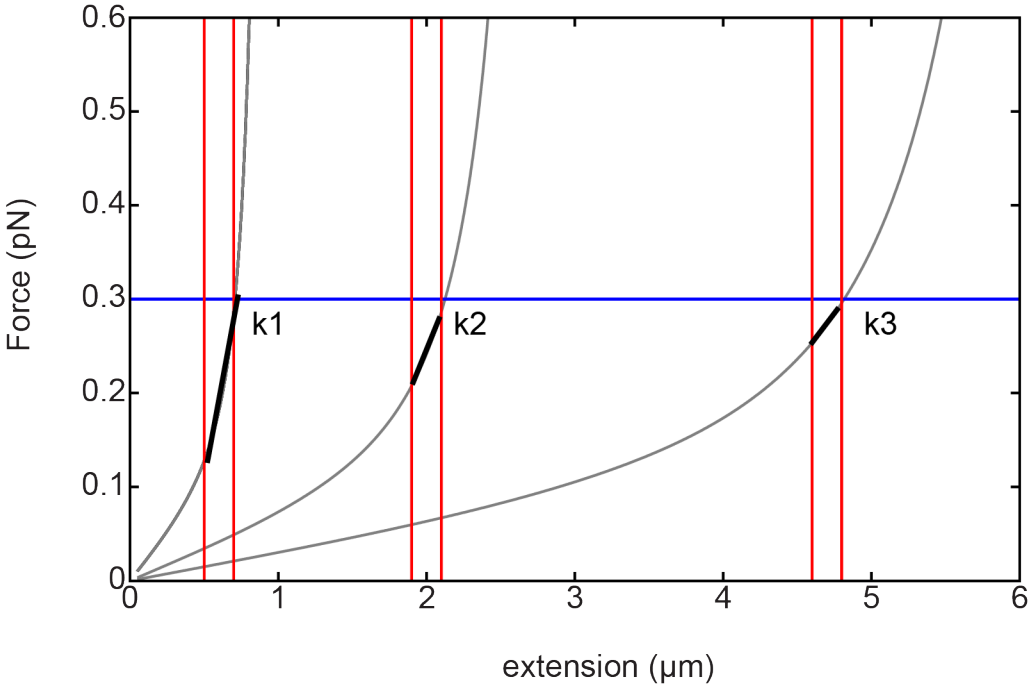

Supplementary Figure S8: Determining the spring constant of the DNA at three compaction states.

Supplementary references

1. Kerssemakers, J. W. J. *et al.* Assembly dynamics of microtubules at molecular resolution. *Nature* **442,** 709–12 (2006).
2. Crut, A., Koster, D. A., Seidel, R., Wiggins, C. H. & Dekker, N. H. Fast dynamics of supercoiled DNA revealed by single-molecule experiments. *Proc. Natl. Acad. Sci. U. S. A.* **104,** 11957–62 (2007).